Scientific Research Publishing

Open Journal of Geology, 2023, 13, 23-50
https://www.scirp.org/journal/ojg
ISSN Online: 2161-7589
ISSN Print: 2161-7570

Application of Vertical Electrical Sounding in Mapping Lateral and Vertical Changes in the Subsurface Lithologies: A Case Study of Olbanita, Menengai Area, Nakuru, Kenya

Daniel Mogaka Nyaberi

Department of Environmental Earth Sciences, University of Eldoret, Uasin Gishu, Kenya
Email: nyaberimogaka@gmail.com

How to cite this paper: Nyaberi, D.M. (2023) Application of Vertical Electrical Sounding in Mapping Lateral and Vertical Changes in the Subsurface Lithologies: A Case Study of Olbanita, Menengai Area, Nakuru, Kenya. *Open Journal of Geology*, **13**, 23-50.
https://doi.org/10.4236/ojg.2023.131002

Received: November 30, 2022
Accepted: January 10, 2023
Published: January 13, 2023

Abstract

Much study has been done in the study area linking Vertical Electrical Sounding (VES) interpreted results to lithologies in the subsurface though only tend to indicate the vertical changes with the aim of mapping the occurrence of groundwater aquifers. Several boreholes have been drilled in the study area, though not much has been done to compare the vertical and lateral lithologic changes in the study area. This research is based on VES modelled geoelectric layers compared from point to point and using borehole logs as control data to establish inferences of certain lithology in the subsurface. The inversion of each VES curve was obtained using an AGI Earth Imager ID inversion automated computer program and resistivities and thicknesses of a geoelectric model were estimated. The analyzed VES data interpretation achieved using the curve matching technique resulted in mapping the subsurface of the area as portraying H-type; $\rho_1 > \rho_2 < \rho_3$, K-type; $\rho_1 < \rho_2 > \rho_3$, A-type; $\rho_1 < \rho_2 < \rho_3$, Q-type; $\rho_1 > \rho_2 > \rho_3$, representing 3-Layer subsurface and subsequently a combination of HK, HA and KHK types of curves representing 4-Layer and 5-Layer in the subsurface. The analysis further deployed the use of the surfer software capabilities which combined the VES data to generate profiles running in the west-east and the north-south direction. A closer analysis of the curve types indicates that there exists a sequence showing a shifting of the order of arrangement between the west and the east fragments which incidentally coincides with VES points 8, 9 and 10 in the West-East profiles. The lateral change is noted from the types of curves established and each curve indicates a vertical change in the subsurface. Control log data of lithologies from four boreholes BH1, BH2, BH3 and BH5 to show a qualification that different resistivity values portent different lithologies. Indeed, an analysis at

borehole BH3 lithologies is dominated by either compacted rocks or soils, insinuating a scenario of compression experienced in this part of the subsurface which confirmed compression of subsurface formations. A correlation of the VES curve types and their change from one point to another in the study area are evident. This change supported by the surfer generated profiles from the modeled VES data show that there exists and inferred fault line running in the north-south in the area. The inferred fault line by VES mapping, is magnificently outlined by the geological map. There is exuded evidence from this study that the application of VES is able to help map the lateral and the vertical changes in the subsurface of any area but the evidence of the specific lithologies has to be supported by availability of borehole log control data. The VES data was able to enumerate vertical layering of lithologies, lateral changes and even mapping vertical fault line in the study area.

Keywords

Curve Matching, Geoelectric Models, Inferred Fault Line, Lithologies, Resistivities

1. Introduction

The response of the earth to the flow of electrical current is the basis of electrical resistivity [1], under which the Vertical Electrical Sounding (VES) is the commonest resistivity field application for conventional examination of the subsurface. As noted by [2], deployment of VES in collection of data is feasible in large areas given the easiness and economical nature of the method. The VES method correlates vertical apparent resistivity with depth of the subsurface [1] in models achieved by the use of collinear configurations and the obtained results can be interpreted to mean overburden thickness, water table depth, the thicknesses and depths of subsurface layers [3]. Similarly, [4], successfully used resistivity in mapping features not observed at the surface like rock types, structural formations and fractures. The subsurface resistivity changes depending on the rock's number of open spaces between particles (porosity), the degree of interconnection of the pores, conductivity of the pore water [5] with fresh compact rocks having relatively higher resistivities compared to saturated sand or gravel [6]. Rigorous work goes unto these VES interpretations, where raw apparent resistivities modelled to give closer to reality (true resistivities), where a close match is attained between the calculated and observed resistivity curves thereafter getting geoelectric layer thicknesses [6].

The resistivity differences basis in VES has been used successfully in delineating the subsurface stratigraphy [7], to the extent of establishing sequences of horizontal or slightly inclined layers with clearly defined thickness and true resistivities [4]. Though, [6] notes that translating the resistivity results into geological senseentails being equipped with knowledge of the characteristic resistiv-

ity values for the different types of subsurface geological materials which can be modelled to the surveyed area. Further evidence in research in Mayo Kani Area in Cameroon by [8], indicates that apparent resistivities were interpreted to give subsurface layers enumerated as topsoil/clayey sand/water sutured sand horizon/bedrock; topsoil/sand/clayey sand/porous or fractured formation; topsoil, clayed sand/aquifer/bedrock intrusion, topsoil/clayey sand/sand/altered granite. Accordingly, [9] has shown that VES is useful in identifying subsurface profiles at least from their work done in volcanic island of Weh, Aceh.

Stratigraphic orders of certain lithologies are evident like the old land surfaces [10] are clearly recognizable in the geological logs at depths range of; 164 - 166 m for BH 1, 184 - 186 m for BH 2, 118 - 132 m and 182 - 188 m for BH 3, 186 - 190 m for BH 4, 106 - 114 m and 206 - 210 m for BH 5, 70 - 76 m for BH 6, 110 - 114 for BH 7, 174 - 180 m for BH 7A and BH 8 at a depth range of 170 - 180 m. Despite the linking of the VES interpreted results to lithologies in the subsurface within the study area, many tend to only indicate the vertical changes which are in most cases linked to occurrence of groundwater aquifers. [6] certainly shows that there is indeed a good correlation in a reference point within the study area, between its VES data and the lithologies extracted from borehole log. [11] in his worknotes that geological mapping, geophysical surveys covering VES as well as electrical resistivity tomography (ERT) and geo-log assessments have extensively been deployed in hydrogeology valuations in the area of interest. The focus of the aquifer lithologies by [2], indeed shows that using the VES data with borehole log as control data, could help to distinguish the main aquifer, related aquifer parameters from other aquifers. Several boreholes have been drilled in the study area, though not much has been done to compare and contrast the vertical and lateral lithologic changes in the study area.

The VES method has been widely used in the study area, mainly investigating subsurface structural orientation, groundwater aspects of quality and quantity, and as such mainly focusing on the aquifers of the area. This study has purposed to evaluate the lithological changes both laterally and vertically using VES as the main method of investigation. The work done in the area through various analyses ([2] [5] [6] & [11]) show possible irregularities in the subsurface of the study area, and thus a program of soundings and the interpretation can help resolve such problems associated with traversing anomalies. This research is based on VES modelled geoelectric layers compared from point to point and using borehole logs as control data to establish inferences of certain lithology in the subsurface.

2. Geology and Hydrogeology

The geology of the Rift is formed of Lava flow rocks whose origin is related to fissures and faulting [6] associated with the formation and subsequent expansion of rift valley. The local geology is represented by lava sheets associated with the eruption of Menengai volcano, whose weathering results unto superficial sediments and soils. The works by [12] and [13] indicate that the geology of the Ol-

banita Menengai area comprises a succession of Miocene-Pleistocene volcanic, mainly phonolites, trachytes and basalts, with pyroclastics and intervening lacustrine beds attributed to the Pleistocene period. [11] further breaks down the lithologies beneath the Olobanita, Kabatini and Baharini based on assessment of borehole geo-logs to top brown soils and sediments (≈ 10 m thick) overlying lava flows of rhyolites, basalts, trachytes or phonolitic trachytes, with thickness ranges 10 - 40 m, with alternating consolidated pyroclastic materials such as tuffs, agglomerates, ashes and their derivatives comprising loose tuffaceous sands or pumiceous gravels. Geological formations have been mapped (**Figure 1**) with some that appear to be on the surface in one point mapped as a subsurface layer in another point of the region occasioned by the tectonic episodes ranging from minor faulting, major faulting, unconformities and warping [6].

Groundwater in the Kenyan Rift Valley occurs in volcanic rocks and at fluctuating depths and several aquifers may exist top of one another [6]. The formations beneath the study area in some instances have a tendency of collapsing during borehole drilling operations [6]. Groundwater occurrences in the area have been innumerably discussed with [2], qualifying that there exist four aquifers beneath the study area which occur in different depths from one borehole to another [11]. The different depths of water strike are probably attributed to the vertical fault displacement due to volcanic eruptive series followed by major faulting in the area [6]. [5] shows that episodic lava and pyroclastic deposits in the area were followed by periods of weathering and erosion. [10] describes these deposits' occurrence in depths beneath the subsurface in the area as channels of water which are accommodated by old land surfaces with [11] defining them as highly conductive coarse sand aquifer layers.

3. Research Methods

3.1. Vertical Electrical Sounding Data Collection

During VES data collection there was an assumption of having uniform one-dimensional layering coupled with progressively increasing layer thicknesses with depth, with smallest to largest, respectively. The Schlumberger (**Figure 2**) array was carefully laid where the AB/2 and MN/2 were geometrically increased thus avoiding crossing resistivity contrasts in the near surface or accommodating the anticipated thickness changes with depth.

With the Schlumberger array, for each measurement the current electrodes A and B are moved outward to a greater separation throughout the survey, while the potential electrodes M and N stay in the same position until the observed voltage becomes too small to measure. Otherwise sometimes there was need to increase the voltage in the settings of the equipment to ensure minimization of noise, and this adjustment automatically adjusts the current into the ground. For checking the reliability of the data, the soundings were interpreted in the field by using curve matching procedures.

where A (C1) and B (C2) are current electrodes, and M (P1) and N (P2) are potential electrodes.

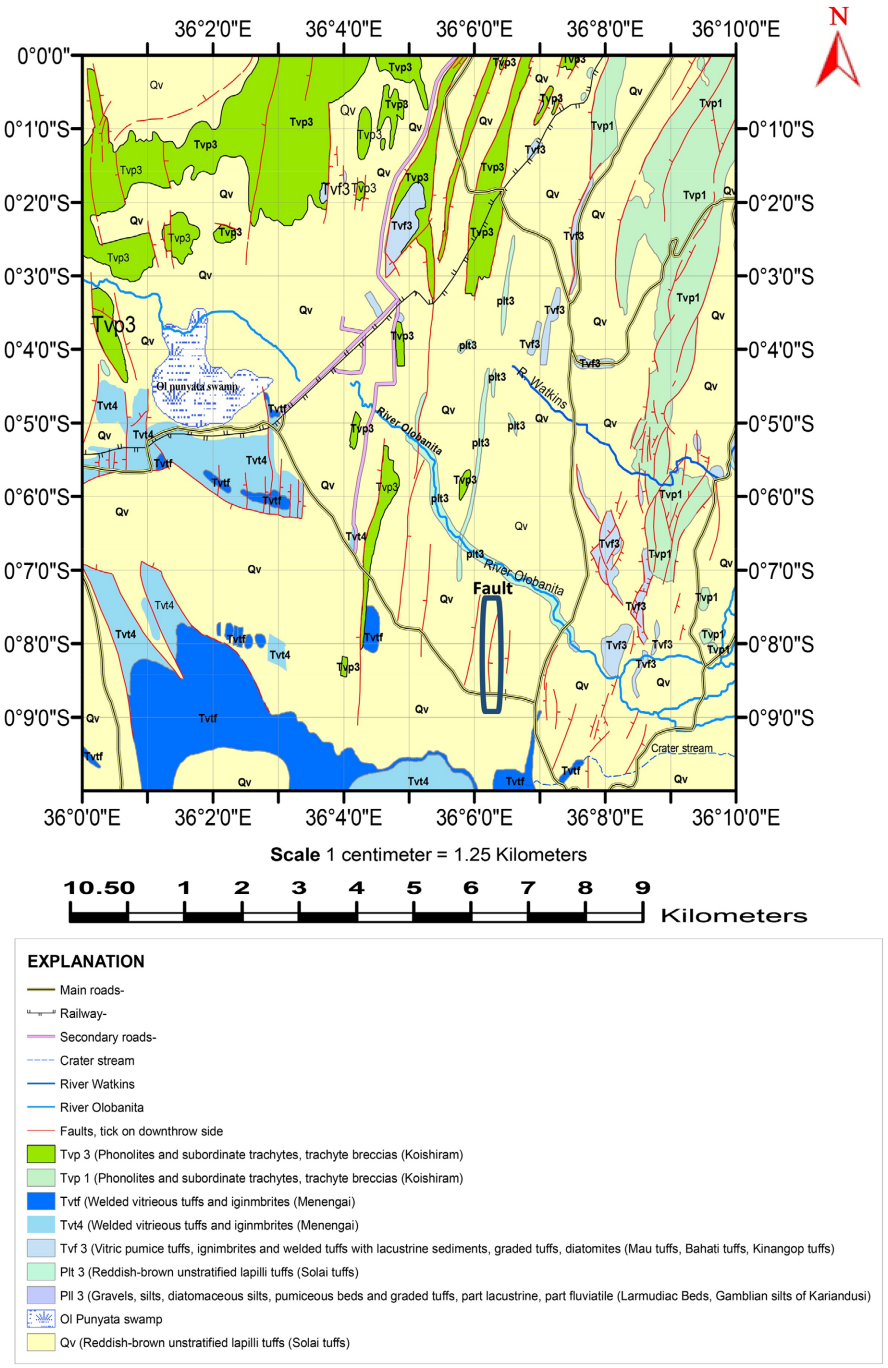

Figure 1. The geological map of the study area.

The process has an assumption that the medium below the sub-surface of the earth is homogeneous and isotropic and considered to have trueresistivity ρ, otherwise normally, the geology is heterogeneous thus its resistivity is presented as apparent resistivity (Equation (1));

$$\rho a = 2\pi \frac{\Delta v}{I} k \tag{1}$$

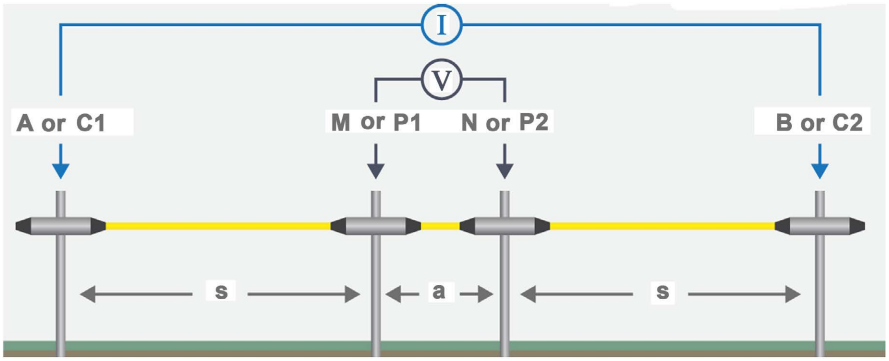

Figure 2. Schlumberger array showing electrodes used to perform VES measurements. (after AGI, accessed Nov 14, 2022).

Two hundred and nine (209) apparent resistivity values in a 100 by 100 meter grid, covering nineteen lines (19) called VES points in the East west direction and eleven (11) lines, otherwise referred to as profiles, in the North-South direction were collected through VES from the Olbanita area (Figure 3).

3.2. Vertical Electrical Sounding Data Processing and Analysis

The Resistivity is automatically measured and calculated giving the heterogeneity of the subsurface lithologies with apparent resistivity (pa) calculated based on I, ΔV, and electrode spacing. The progressive increase of AB/2 results in a generation of resistivity-depth relationship. Data Processing and analysis were achieved in a multipronged approach. The data presented as apparent resistivity by the equipment is achieved by the internal data processing based on the Schlumberger array. This first phase was digitally achieved with the Terrameter's data handling internal capabilities considering the instructions keyed into the equipment when collecting the data supported by the Shlumberger protocol installed in the Terrameter. The AGI Earth Imager ID inversion automated computer program used in data analysis requires data in the format $\Delta V/I$ thus requiring conversion of the apparent resistivity data before it could be used in determination of the actual resistivities, thickness and depth of the various geoeletrical layers. The $\Delta V/I$ processed data was input into a format used by the AGI Earth Imager 1D inversion software and the datasets were read by the software which in turn gave the log-log plot of the data and the initial model.

The inversion of each VES curve was obtained using an AGI Earth Imager ID inversion automated computer program. The inversion method modifies the initial model until a very close match between the calculated and the measured resistivity curves was obtained. Based on these interpretations, apparent resistivities and thicknesses of geoelectric layers from models thought to be closer to reality, were estimated, and modified by trial and error until a very close match was attained between the calculated and observed resistivity curves. Accordingly, the automatic curve-matching computer program results in a geoelectric model affirmed when the calculated apparent resistivity matches the given field curve almost exactly. Thus, the interpretation as determined by the program is

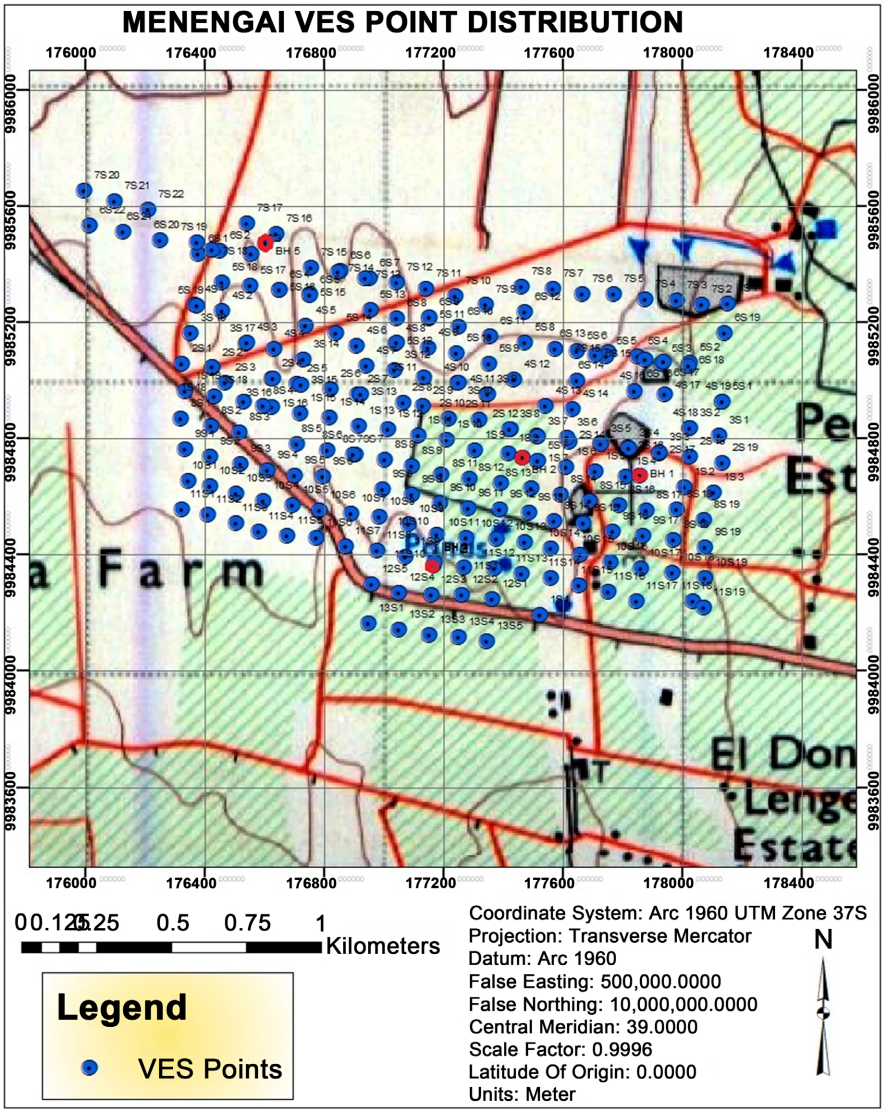

Figure 3. Map showing VES data collection points in the study area.

mathematically correct but may not necessarily correspond to lithological reality. The number of layers as determined by the program are geoelectric rather than lithologic, and the resistivities of some of these layers are sometimes unrealistically small or large, while their thicknesses are too small to be detected by the VES method. In other words, the results may, on some occasions, tend to exceed the limitations of the VES method.

4. Results

The data were processed using excel to convert them into the required *V*/*I* statistics. The data were analyzed by using the AGI Earth Imager ID inversion software to obtain the true resistivity values through the inversion modelling. The inversion procedure resulted into both modelled curves and corresponding modelled resistivity values which were then analysed further through plotting using surfer software. The use of surfer helped by combining several points in a straight

line considering the depth (X-values), the horizontal (Y-values) and the resistivity values with depth (Z-values), whose consequence was a vertical and lateral correlation between the points. The analyzed VES data interpretation using the curve matching technique that is, the comparison between the standard curves and the inversely generated VES curves was carried out. The curves are based on a three-layered earth classified into H, K, A and Q type curves, based on shape, where their correlation with apparent resistivity they are given as: H-type; $\rho_1 > \rho_2 < \rho_3$, K-type; $\rho_1 < \rho_2 > \rho_3$, A-type; $\rho_1 < \rho_2 < \rho_3$, Q-type; $\rho_1 > \rho_2 > \rho_3$, and subsequently a combination of the above is used to represent several layers in the subsurface.

There are dominantly H-K and K types of curves in the study areas as presented in the analyzed summarized in Table 1, with exceptions of one type Q, one type H, three type A, two of combined type K-H-K and one of combined type HA. Further results are adduced using geologic logs as control data using four different boreholes drilled in the area in comparison with the VES data collected and analyzed from these points (Tables 2-5).

Accordingly these curves (Table 1) are conspicuously aligned to specific profiles (Figures 4(I)-(XI)) running in the north-south direction in the field with each having nineteen VES points. Given the consistency observed in the arrangement of the curves in relation to profiles in the west-east (VES 1 - 19) direction, further analysis reveals several uniformity, but the variations are noted too. The arrangement of the profiles in the field appears in the order 7, 6, 5, 4, 3, 2, 1, 8, 9, 10 and 11 (Figure 3), and thus in the presentations, and further analysis, an order of 1(7), 2(6), 3(5), 4(4), 5(3), 6(2), 7(1), 8, 9, 10, 11 has been adopted (see Table 1 and Figures 4(I)-(XI)). Profile-wise, in profile 1(7) the analysis is given as eight combined type H-K curves starting from the west (VES 1 - 7, 10) of the profile and eleven type K curves at VES points 8, 9, 11 - 19 in the eastern section. Profile 2(6) in the west-east direction has five type K curves (VES 1, 2, 4 - 6), three type A curves (VES 3, 7, 8), one type Q curve (VES 9), one combined type K-H-K (VES 10), with seven combined type H-K curves (11 - 14, 16 - 18), one type H (VES 15) and one combined type H-A (VES 19). In Profile 3(5) there are seven combined type H-K curves (VES 1, 3 - 8), one combined type K-H-K (VES 2) and eleven type K curves (VES 9 - 19). Profiles 4(4) and 5(3) presents one type K curves, in the west-east (VES 1 - 19) direction. There is a clear demarcation shown in profile 6(2) with nine type K curves (VES 1 - 9), eight combined type H-K curves (VES 11, 12, 14 - 19), with exceptions of combined type H-A at VES 10 and type A at VES 13. Profile 7(1) has nine combined type H-K curves (VES 1 - 9) and ten type K curves (VES 10 - 19). The profiles eight to eleven shows uniformity in the west to east direction, with all having type K curves. Surfer 2D plots (Figures 4(I)-(XI)) were generated from VES data, where the profiles are numbered north-south with each having nineteen (19) VES points except profiles 1(7) and 2(6) with twenty two (22) VES points each.

The analysis further deployed the use of the surfer software capabilities, combined the VES data (VES 1 - 19) for every profile and thus accounting for eleven

Table 1. Showing field orientation of surfer profiles with their VES points assigned the types of curves match they represent.

	Profiles arranged N-S	1 (7)	2 (6)	3 (5)	4 (4)	5 (3)	6 (2)	7 (1)	8	9	10	11
VES No. in W-E per Profile	Meters	0	100	200	300	400	500	600	700	800	900	1000
1	0	HK	K	HK	K	K	K	HK	K	K	K	K
2	100	HK	K	KHK	K	K	K	HK	K	K	K	K
3	200	HK	A	HK	K	K	K	HK	K	K	K	K
4	300	HK	K	HK	K	K	K	HK	K	K	K	K
5	400	HK	K	HK	K	K	K	HK	K	K	K	K
6	500	HK	K	HK	A	K	K	HK	K	K	K	K
7	600	HK	A	HK	K	K	K	HK	K	K	K	K
8	700	K	A	HK	K	K	K	HK	K	K	K	K
9	800	K	Q	K	K	K	K	HK	K	K	K	K
10	900	HK	KHK	K	K	K	HA	K	K	K	K	K
11	1000	K	HK	K	K	K	HK	K	K	K	K	K
12	1100	K	HK	K	K	K	HK	K	K	K	K	K
13	1200	K	HK	K	K	K	A	K	K	K	K	K
14	1300	K	HK	K	K	K	HK	K	K	K	K	K
15	1400	K	H	K	K	K	HK	K	K	K	K	K
16	1500	K	HK	K	K	K	HK	K	K	K	K	K
17	1600	K	HK	K	K	K	HK	K	K	K	K	K
18	1700	K	HK	K	K	K	HK	K	K	K	K	K
19	1800	K	HA	K	K	K	HK	K	K	K	K	K

Table 2. Profile 8 VES 17 Analyzed data compared with borehole 1 geologic log (VES done near BH1).

VES modeled Depth (m)	Log depth (m)	Resistivity (Ωm)	Lithology
0 - 7.144	0 - 2	40.381	Reddish brown top soil
7.144 - 17.159	2 - 30	68.105	Loose gravel (highly weathered)
17.159 - 25.903		700.217	
25.903 - 37.542		624.657	
37.542 - 47.371	30 - 68	236.907	Very hard phonolytic tuffs
47.371 - 59.263		111.019	
59.263 - 73.653	68 - 70	50.436	Reddish soil
73.653 - 91.064	70 - 86	27.708	Dust
	86 - 94		Dark grey pumiceous rock

Continued

	94 - 104		Brownish tuff (highly weathered)
91.064 - 112.132	104 - 106	20.43	Dark grey pumiceous rock
	106 - 112		Brownish tuff (highly weathered)
	112 - 116		Greyish phonolytic tuffs
112.132 - 124.272	116 - 118	42.712	Fine grained sand
	118 - 130		Dark grey pumiceous tuffs
124.272 - 152.313	130 - 140	25.204	Loose gravel (reddish and grey pebbles)
	140 - 152		Weathered grey tuffs
152.313 - 168.47	152 - 164	53.938	Dark grey tuffs
	164 - 166		Reddish brown soil
	166 - 174		Dark grey tuffs (fine grained)
168.47 - 205.794	174 - 194	38.885	Dark grey pumiceous tuffs
	194 - 200		Compact phonolytic tuffs
	200 - 204		Dark grey phonolites
	204 - 218		Greenish tuffs
205.794 - 227.299	218 - 220	56.775	Grey fine grained sand
	220 - 234		Reddish soil
227.299 - 250.955	234 - 242	53.24	Loose sediments with red stains
	242 - 256		Brownish tuffs
250.955 - 305.6	256 - 260	45.278	Greenish trachytes
	260 - 270		Brownish tuffs

Table 3. Profile 8 VES 13 Analyzed data compared with borehole 2 geologic log (VES done near BH2).

VES modeled Depth (m)	Log depth (m)	Resistivity (Ωm)	Lithology
0 - 7.144	0 - 12	39.41	Brown silty top soil
7.144 - 17.159	12 - 22	121.2	Greyish brown tuffs
17.159 - 25.903	22 - 32	437.348	Brown tuffs
25.903 - 37.542		679.722	
37.542 - 47.371	32 - 48	384.732	Light grey trachytes
47.371 - 59.263	48 - 52	214.932	Light brown tuff
59.263 - 73.653	52 - 70	97.765	Grey trachytes
	70 - 72		Weathered trachytes
	72 - 76		Yellow tuffs
73.653 - 91.064	76 - 86	43.083	Brownish red silty clay
	86 - 90		Greyish weathered trachytes

Continued

91.064 - 112.132	90 - 100	24.062	Fresh trachytes
	100 - 118		Pumice trachytes
112.132 - 124.272	118 - 120	42.843	Highly pumiceous trachytes
124.272 - 152.313	120 - 140	22.017	Fresh trachytes
	140 - 150		Pumice trachytes
	150 - 154		Highly pumiceous trachytes
152.313 - 168.47	154 - 158	50.643	Grey pumiceous trachytes
	158 - 162		Angular agglomerates
	162 - 182		Dark grey trachytes with quartz
	182 - 184		Yellowish greyish weathered trachytes
168.47 - 205.794	184 - 186	32.191	Red silty soil
	186 - 204		Dark brown trachytes
	204 - 206		Greyish green tuffaceous trachytes
	206 - 208		Yellowish grey sediments
205.794 - 227.299	208 - 218	54.358	Brownish sediments with tuffs
	218 - 226		Dark brown compact tuffs
227.299 - 250.955	226 - 232	48.051	Brownish phonolites
	232 - 240		Trachytic tuffs
	240 - 246		Black phonolites
	246 - 248		Brownish grey tuffs
	248 - 254		Dark greyish phonolytic trachytes
250.955 - 305.6	254 - 258	35.057	Trachytic tuffs
	258 - 264		Greenish grey trachytic tuffs
	264 - 268		Dark grey trachytes
	268 - 271		Fractured phonolytic trachytes

Table 4. Profile 11 VES10 Analyzed data compared with borehole 3 geologic log (VES done near BH3).

VES modeled Depth (m)	Log depth (m)	Resistivity (Ωm)	Lithology
0 - 7.144	0 - 8	65.615	Reddish brown top soil
7.144 - 17.159	8 - 34	100.994	Pyroclastic agglomerates, mainly of grey trachytes
17.159 - 25.903		184.283	
25.903 - 37.542		488.836	
37.542 - 47.371	34 - 60	479.781	Compact phonolitic trachytes
47.371 - 59.263		453.513	
59.263 - 73.653	60 - 76	367.071	Compact phonolitic tuffs

Continued

73.653 - 91.064	76 - 80	282.482	Greyish volcanic ash,
	80 - 86		Reddish brown soil (old land surface)
	86 - 92		Compact greyish phonolitic trachytes
	92 - 98		Light grey pumiceous tuffs
91.064 - 112.132	98 - 106	210.026	Grey tuffs
	106 - 118		Dark grey pumiceous tuffs
112.132 - 124.272	118 - 132	180.698	Reddish brown soil (old land surface)
	132 - 142		Greyish clay
124.272 - 152.313	142 - 146	139.566	Compact phonolitic trachytes
	146 - 156		Grey clay
152.313 - 168.47	156 - 176	138.866	Fissured phonolitic trachytes
	176 - 182		Grey pumiceous tuffs
168.47 - 205.794	182 - 188	101.449	Brownish soil
	188 - 192		Grey pumiceous tuffs
	192 - 202		Brownish soil
205.794 - 227.299	202 - 218	119.462	Grey pumiceous tuffs
227.299 - 250.955	218 - 242	95.588	Weathered phonolitic tuffs
	242 - 248		Grey tuffs
250.955 - 305.6	248 - 265	30.269	Dark grey phonolitic trachytes

Table 5. Profile 1(7) VES 16 Analyzed data compared with borehole 5 geologic log (VES done near BH5).

VES modeled Depth (m)	Log depth (m)	Resistivity (Ωm)	Lithology
0 - 7.144	0 - 2	172.803	Brownish top soil
7.144 - 17.159	2 - 16	227.347	Brownish pebbles
17.159 - 25.903	16 - 22	565.888	Reddish grey pumiceous tuffs
	22 - 24		Greyish pebbles of tuffs
25.903 - 37.542	22 - 32	1162.001	Grey compact phonolites
	32 - 40		Grey pumice
37.542 - 47.371	40 - 52	634.405	Greyish compact phonolitic trachytes
47.371 - 59.263	52 - 54	304.985	Fine light grey pumice
59.263 - 73.653	54 - 64	154.96	dust
73.653 - 91.064	64 - 96	104.022	Grey phonolites
91.064 - 112.132	96 - 100	92.73	Dark grey fine grains of pumice
	100 - 106		Reddish brown tuffs
	106 - 114		Red silt soils

Continued

112.132 - 124.272	114 - 122	149.376	Grey tuffs
124.272 - 152.313	130 - 150	98.635	Grey compact phonolites
152.313 - 168.47	150 - 154	153.876	Dark grey phonolitic tuffs
	154 - 176		Greenish trachytic phonolites
	176 - 182		Greenish grey trachyte
	182 - 184		Dark grey phonolites
168.47 - 205.794	184 - 188	102.788	Weathered tuffs with red particles
	188 - 196		Greenish tuff
	196 - 206		Pumice with fine particles
	206 - 210		Reddish brown silt
	210 - 214		Grey soft tuffs
205.794 - 227.299	214 - 218	130.729	Greenish tuffs
	218 - 222		Grey tuffs
	222 - 224		Weathered brownish tuffs
227.299 - 250.955	224 - 238	97.6	Weathered light green tuffs
	238 - 250		Grey phonolitic tuffs
	250 - 252		Dark grey pumice
250.955 - 305.6	252 - 265	70.137	Grey phonolitic trachytes
	265 - 270		Brownish clay

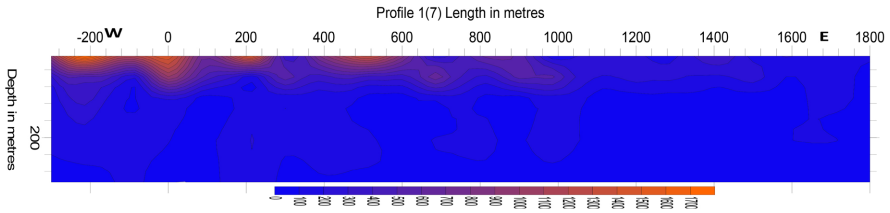

(I)

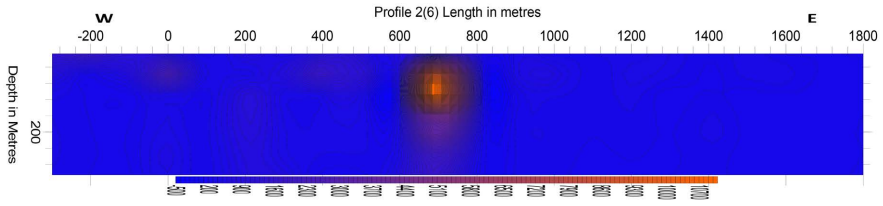

(II)

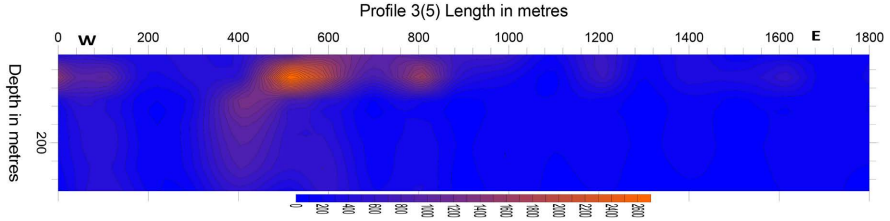

(III)

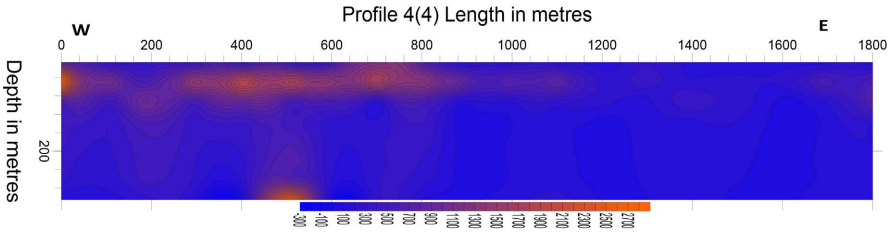

(IV)

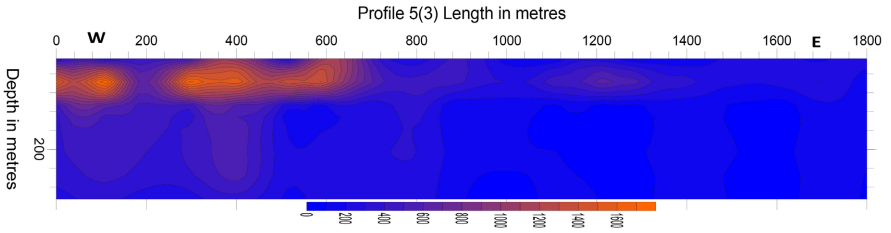

(V)

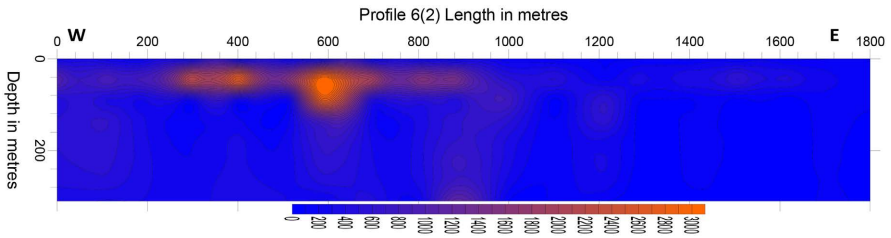

(VI)

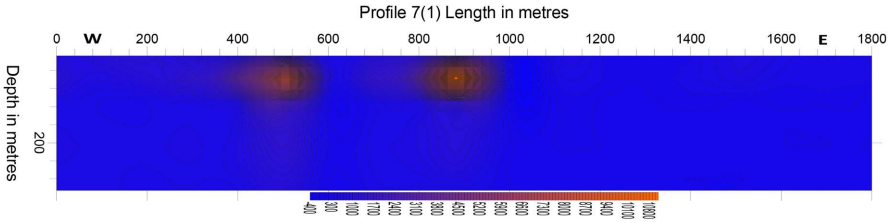

(VII)

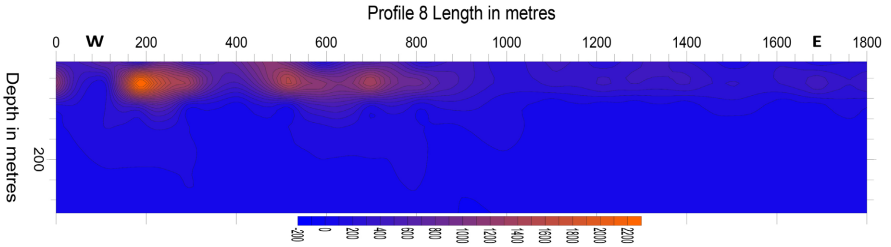

(VIII)

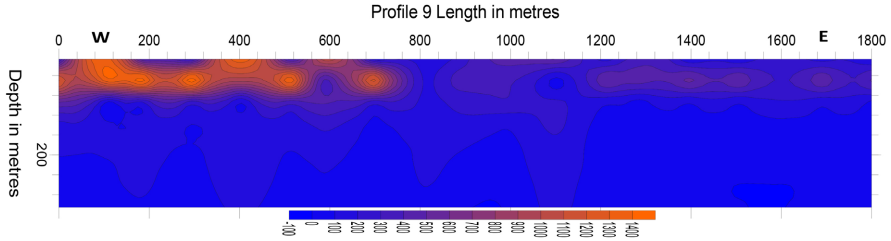

(IX)

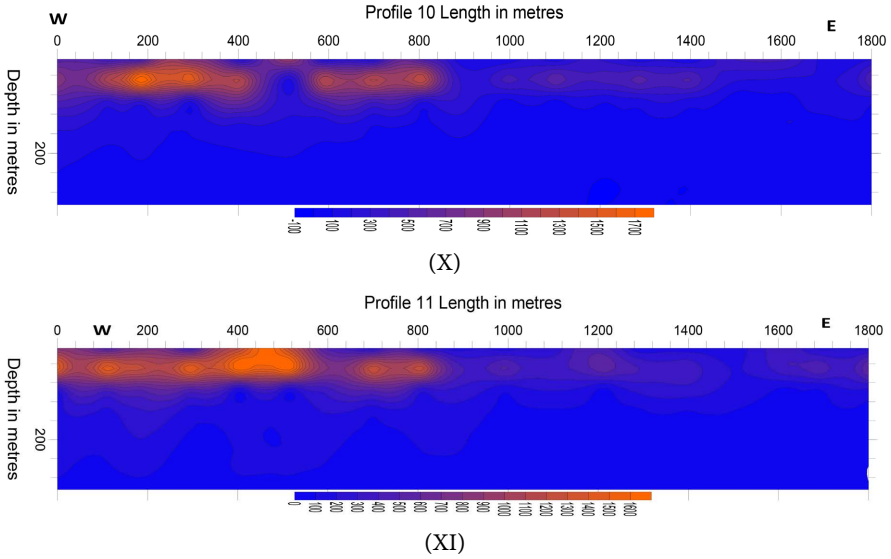

Figure 4. (I)-(XI). Surfer Profiles of combined horizontal VES points' (at 100 m separation) f modelled resistivity data.

profiles (1(7) to 11). The points where VES data were collected are shown in **Figure 3** showing the lines (VES points) in the west-east direction and the profiles in the north-south direction. The generated profiles have a length of 1800 meters (at 100 meter spacing) covering nineteen VES points, except profiles 1(7) and 2(6) with length of 2100 meters (with 22 VES points each) as shown in **Figures 4(I)-(XI)**. All the VES points have an equal depth consideration of 305.60 meters determined from the maximum spacing AB/2 of 320 meters and MN/2 of 25 meters , and considering a depth factor of 2.5 in the AGI Earth Imager ID inversion software. This depth factor was deployed and was precise in determining the exact geoelectric depths which perfectly translated unto specific depths determined by borehole log data.

Further extracts have been made on the curve types to try and show the differences existing between the shapes of same curve types given in Profile 4(4) as shown in **Figure 5** and **Figure 6**, which shows transition in the west-east direction at VES 8 and VES 9 along the profile. Further correlation is made in appendix **Figure A2** and **Figure A3**.

5. Discussion

The VES curves (**Table 1**) achieved in the study area varies from the 3-layer (A, H, K and Q types), to 4-layer (H-A and H-K) types and 5-layer (K-H-K) types. The dominance in occurrence can be determined by percentages of the 3-layer A type at 1.44 percent, H type at 0.48 percent, K type at 76.55 percent and type Q at 0.48 percent. The 4-layer curve represented by HK has18.66percent representation and 0.96 for HA type, and 5-layer curve of KHK with 0.48 percent. This analysis in itself indicates that in the area of 1.8 square kilometers there exists curves portraying several subsurface layers. A closer check at the curve types in

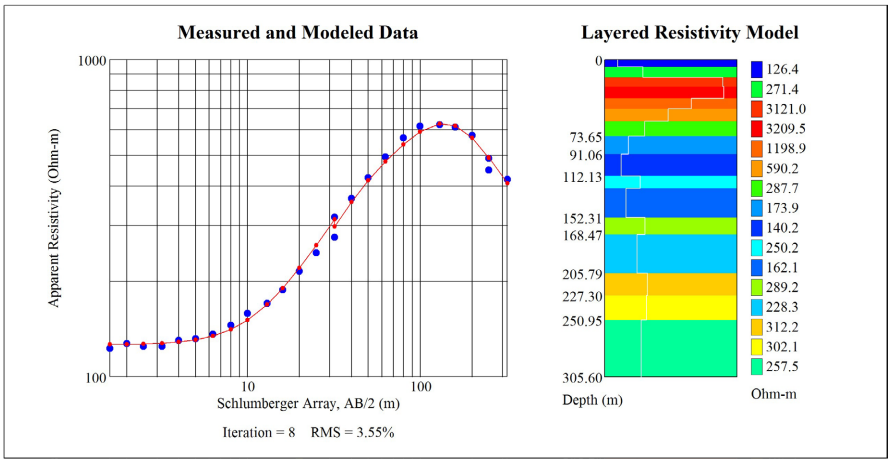

Figure 5. Profile 4(4) VES 8 showing measured (blue dots) and modeled (red line and dots) VES data.

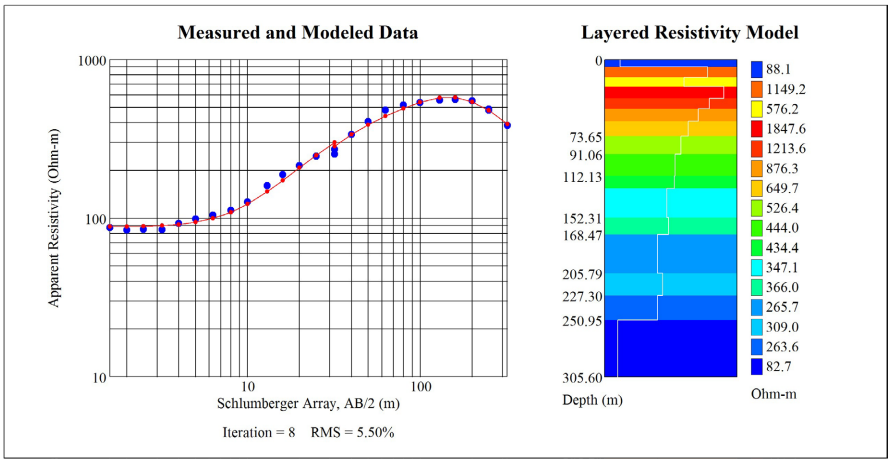

Figure 6. Profile 4(4) VES 9 showing measured (blue dots) and modeled (red line and dots) VES data.

their appearance in the profiles (**Table 1**), there too exists a sequence showing a shifting of the order of arrangement. For example, the profiles 1(7), 2(6), 3(5), 6(2) and 7(1) evidently show shifting at about VES points 8, 9 and 10, from either 3-layer to 4-layer or vice versa. The lateral change is noted from the curves as shown by the number of layers, and basically happens at a point diving VES 8 and VES 9 (**Table 1**, and **Figure 5** and **Figure 6**). The shape of the K type curves of VES points 1 - 8 are different (**Figure 5**; appendix **Figure A2**) from the VES point curves 9 - 14 (**Figure 6**; appendix **Figure A3**), indicating that though profile 4(4) is represented by K type curve, the resistivities' values vary where the VES points 1 - 8 having their curves starting at above 100 Ωm, while for VES points 9 - 19 starting below 100 Ωm.

There are differences equally picked in the surfer plotted profiles, where heterogeneity is observed in the mapped subsurface. The different resistivity values' merging is achieved between the points lengthwise in each profile, carrying out gridding method with minimum curvature using a banding of 100 Ωm. Each of

the VES point has a depth of 305.6 meters, giving a two dimensional profile along nineteen (19) points in 100 meter separation (1800 by 305.6 meters) and this subsequently shows the changes both vertically and laterally. A keen check in **Figures 4(I)-(XI)**, there exists a feature Y mapped between lengths 1600 and 1700 meters in all profiles except blockage by orientation of feature X witnessed at profiles 4(4), 5(3) and 6(2). In the North-South profiles of 16 NS and 17 NS shown in appendix, **Figure A1**, the feature appears as a tunnel well mapped with resistivities of below 100 Ωm from the depth of approximately 80 meters to beyond the mapped depth of 305.60 meters. These 16 NS and 17 NS profiles match with lengths 1600 meters and 1700 meters in profiles running west to east in **Figures 4(I)-(XI)**. This is evident that VES has a capability of mapping the vertical and lateral changes in the subsurface.

There is noted shift of the subsurface formations at least from the curve types (**Table 1**) where profiles 1(7), 2(6), 3(5), 6(2) and 7(1) have their curves in the VES points for one to about eight, nine or ten being different from those from nine, ten or eleven up to nineteen. Profile 1(7) records H-K type curve at VES points 1 - 7, and 10, and the rest being curve type K at 8, 9 and 11 - 18, with the drift observed at VES 10. This is an indication that on the same line traversing an area measuring 1800 meters , there occurs a change at 600 meters , in the number of curve type determined layers from 4-Layer to 3-Layer. A similar change is evident in the surfer profile 1(7) (**Figures 4(I)-(XI)**) where the constriction of the modeled resistivity values' lines up to 80 meters deep changes at 1000 meters in the west-east direction.

The analysis of Profile 2(6) shows a change transiting from VES 7 - 10 from curves K to HK through A, Q and KHK curves (**Table 1**) and this is a distance of about 300 meters shift from 600 to 900 meters along the line in the west-east direction. This is from 3-Layer through a 5-Layer to 4-Layer curve. The intensity of the involved changes are outstanding in surfer profile 2(6) (**Figures 4(I)-(XI)**) where the modeled resistivity values' line constriction is amplified between 600 meters to 800 meters as compared to the other parts of the profile. There is noted lateral change of resistivities from the outer (600 meter point and 800 meter point) ranks to the centre (700 meter point) as shown in the surfer profile 2(6) (**Figures 4(I)-(XI)**). Though less intense, changes in profile 3(5) move from curves HK to curve K at VES points 8 and 9 (**Table 1**). As is the case with unnoticeable transitional change in the curves but rather sudden, so is the same with the surfer profile 3(5) (**Figures 4(I)-(XI)**) from line 700 meter and 800 meter. Though there isn't change in the curve type in profile 4(4), a closer examination show a change in curves' shapes as shown in **Figure 5** and **Figure 6**. The change happensat 700 meter point in the west-east direction of the profile, showing the possible north-south shifting of the subsurface. The surfer profile 5(3) shows a transition observed at 900 meter where beyond a depth of 100 meters, the VES modeled resistivities are more than 200 Ωm from VES 1 to VES 9, with VES 10 to VES 19 having less 200 Ωm in similar depths.

The drifting for profile 6(2) happens at VES points 9, 10, 11 from curve K to

combined curves H-A and finally to combined curves HK as shown in Table 1 with transition happening at VES point 10 (900 meter point on the profile) shown in surfer profile (Figures 4(I)-(XI)). This transition point exhibit highest resistivity valued feature vertically oriented and obvious in the depths of about 80 meters the considered depth of 305.60 meters. Equally evident for profile 7(1) at VES points 9 and 10 there is a change from combined curve H-K to curve K. Similarities between the drifting in curves and changes in the surfer profile 7(1) are eminent and indicates points of drifting or otherwise called transition.

The VES method has successfully been used in mapping subsurface changes as evidently shown both laterally and vertically using the types of curves (Table 1) and the differences in profiles (Figures 4(I)-(XI)). The vertical variations are attributed to changing lithologies with depth in a particular VES point, as can be shown in the control points done using boreholelogs (Tables 2-5). Notably the boreholes 1 and 2 happen to fall within the same profile 8 separated by about 400 meters, in VES points 17 and 13 respectively. Both the VES modeled curves are 3-Layer type K, shown in same uniformity in subsurface surfer image and are located to the east of the inferred line of transition in the generally noted trends of VES curve types and surfer profiles. In terms of borehole log lithology, there are noted differences in depth between the two boreholes but equally the resistivity modeling has assigned different values to different lithologies. At a depth of about 80 meters in the surfer profile, a similarity between the BH1 and BH2 is picked in terms of modeled resistivity layers, whose further examination of the specific lithologies (Table 2 and Table 3), same similarities are picked where BH1 has dust underlain by dark grey pumiceous rock and BH2 has brownish red silty clay overlying the greyish weathered trachytes. The logs of the two boreholes (BH1 and BH2) show similarities and minimal differences in the lithologies with depth and equally to their point comparison in the modeled resistivity surfer profile and of course with agreeing VES curve type.

The borehole BH3 has its lithologic log given in Table 4 and it is located at the transition boundary at Profile 11 VES 10 and the correlated VES curve is type K. The lithologies are dominated by either compacted rocks or soils, insinuating a scenario of compression experienced in this part of the subsurface. This is augmented by the transition noted in Table 1 and modeled resistivity at VES point along the profile (Figures 4(I)-(XI)) which is the starting point of increasing resistivities from the relatively low values in the Eastern part of the deciphered transition boundary and the increased values in the western part. The expose by borehole BH5 shows a good correlation between the modeled resistivity values and the specific lithologies within the interrelated depths. There is specific distinction between the subsurface modeled resistivity values associated with boreholes BH1 and BH2 found in the eastern part of the demarcated area of transition and the modeled resistivity values of boreholes BH3 and BH4 in the western fragment. A correlation of the VES curve types and their change from one point to another in the study area (Table 1) supported by the surfer generated profiles from the modeled VES data (Figures 4(I)-(XI)) shows that there exists and in-

ferred fault line running in the north-south covering about 300 meters at least. The fault line exists in the subsurface and inferred by VES mapping, it is magnificently outlined by the geological map, shown encircled in a blue vertical rectangle (**Figure 1**). A further evidence is given in the surfer profiles (Appendix, **Figures A1(1)-(19)**) where those in the east (profiles 12 NS to 19 NS) of the inferred fault line are displaying a relatively top to bottom layering and those in the western (Profiles 1 NS to 11 NS) part of the fault line showing a side to side layering.

6. Conclusion

There is exuded evidence from this study that the application of VES is able to help map the lateral and the vertical changes in the subsurface of any area but the evidence of the specific lithologies has to be supported by availability of borehole log control data.VES data collected was modeled using the AGI Earth Imager ID inversion automated computer program and VES curve types were generated. The evaluation of the curves portrayed the existence of 3-layer, 4-Layer and 5-Layer, but also exposed a transition point where the curves were changing. Further analysis using surfer profiling confirmed the departure/transition area which was established to be a fault line through the further analysis of the borehole logs and the area geological map.

Acknowledgements

Special appreciation is given to Water Resources Authority, Kenya, for facilitating me with requested data and the technicians who were crucial in field data collection. Equally acknowledgement goes to the Ministry of Petroleum and Mining, Kenya from whom geological and topographic maps were obtained, which were useful in production the final geological map of the area. I also wish to recognize the prayers, efforts, encouragement, humour and cooperation received from my wife Lydia Gesare and our Children (Amygrace Kerubo Tsitsi, Merrybell Meita, and Madiba Mandela) in the entire period of this research. They allowed me use the meagre family resources for the research and am dearly indebted.

Conflicts of Interest

The author declares no conflicts of interest regarding the publication of this paper.

References

[1] Cardimona, S. (2002) Electrical Resistivity Techniques for Subsurface Investigation. Lecture notes, University of Missouri-Rolla, Rolla.

[2] Nyaberi, D.M. (2022) Determination of the Aquifer and Its Hydraulic Parameters Using Vertical Electrical Sounding, Borehole Log Data and Borehole Water Conductivity: A Case Study of Olbanita Menengai Area, Nakuru, Kenya. *Journal of Geoscience and Environment Protection*, **10**, 204-224. https://doi.org/10.4236/gep.2022.1011014

[3] Nyaberi, M.D. (2020) Delineation of Groundwater Potential Zones in Arid and Semi-Arid Lands Using Integrated Approaches of Remote Sensing, Geophysical Techniques and Borehole Data: A Case Study from Turkana South Sub-County, Kenya. PhD Thesis, Kisii University, Kisii.

[4] Adagunodo, T.A., Sunmonu, L.A., Ojoawo, A., Oladejo, O.P. and Olafisoye, E.R. (2013) The Hydro Geophysical Investigation of Oyo State Industrial Estate Ogbomosho, Southwestern Nigeria Using Vertical Electrical Soundings. *Research Journal of Applied Sciences, Engineering and Technology*, **5**, 1816-1829. https://doi.org/10.19026/rjaset.5.4944

[5] Kuria, Z.N. (2006) Hydrogeology Notes. Lecture notes, University of Nairobi, Nairobi.

[6] Nyaberi, M.D. (2010) Geophysical Characterization of the Lithology and Structure of the Olobanita Well Field, Lower Lake Baringo Basin, Kenya Rift: Implication on Groundwater Occurrence. MSc Thesis, University of Nairobi, Nairobi.

[7] Mohammed, G. and Ibrahim, A. (2014) Geo-Electrical Data Analysis to Demarcate Groundwater Pocket Zones in Kaltungo and Environs, North-Eastern Nigeria. *International Journal of Engineering and Applied Sciences*, **4**. https://doi.org/10.9790/0990-0234350

[8] Kana, J.D., Djongyang, N., Dadjé, A. and Raïdandi, D. (2015) Vertical Electrical Soundings for Subsurface Layers and Groundwater Investigations in the Mayo Kani Area in Cameroon. *International Journal of Science and Research*, **4**, Article ID: SUB151173.

[9] Marwan, M., Rifqan, R., Syafrizal, I. and Muhammad, Y. (2019) Application of Vertical Electrical Sounding for Subsurface Profiling in Weh Island, Aceh Province. *Aceh International Journal of Science and Technology*, **8**, 29-34. https://doi.org/10.13170/aijst.8.1.12879

[10] Sosi, B. (2020) Hydraulic Characteristics of Olbanita Aquifer System in Lower Baringo Basin of the Rift Valley of Kenya: Implications on Groundwater Yields. PhD Thesis, Kisii University, Kisii, 303 p.

[11] Olago, D.O. (2018) Constraints and Solutions for Groundwater Development, Supply and Governance in Urban Areas in Kenya. *Hydrogeology Journal*, **27**, 1031-1050. https://doi.org/10.1007/s10040-018-1895-y

[12] McCall, G.J.H. (1967) Geology of the Nakuru: Thompson's Falls-Lake Hannington Area. Geological Survey of Kenya, Nairobi, 122 p.

[13] Baker, B.H., Mitchell, J.G. and Williams, L.A.J. (1988) Stratigraphy, Geochronology and Volcano-Tectonic Evolution of the Kedong-Naivasha-Kinangop Region, Gregory Rift Valley, Kenya. *Journal of the Geological Society of London*, **145**, 107-116. https://doi.org/10.1144/gsjgs.145.1.0107

Appendix

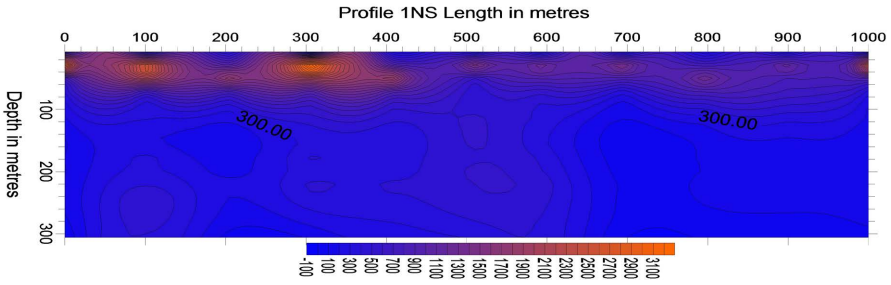

(1)

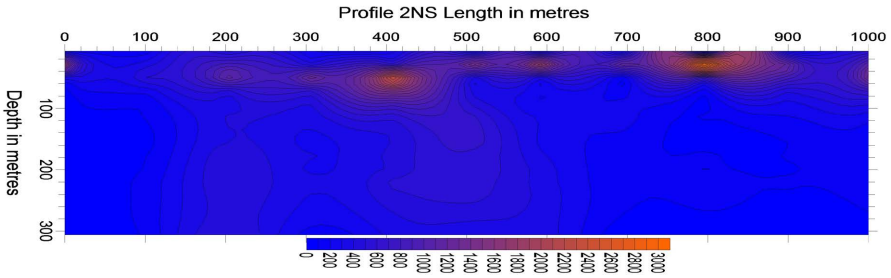

(2)

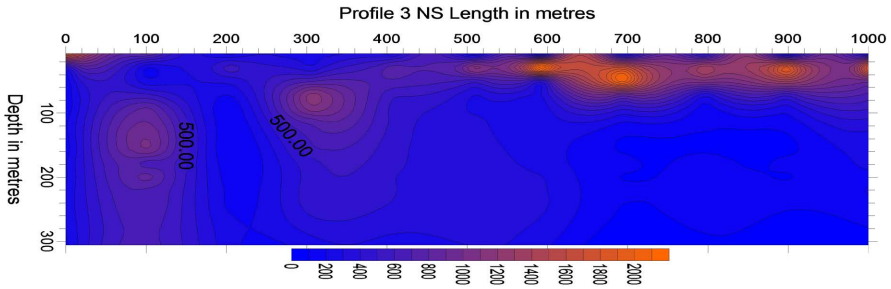

(3)

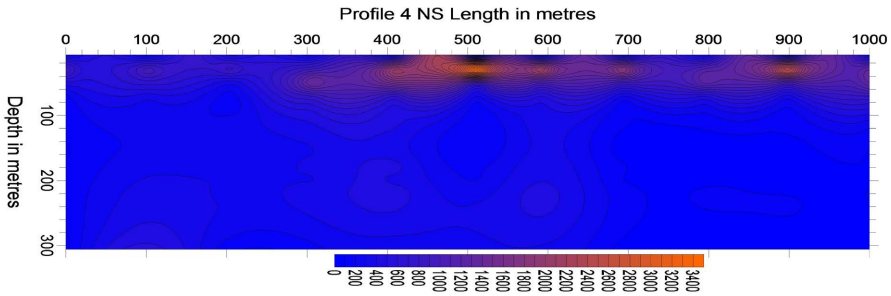

(4)

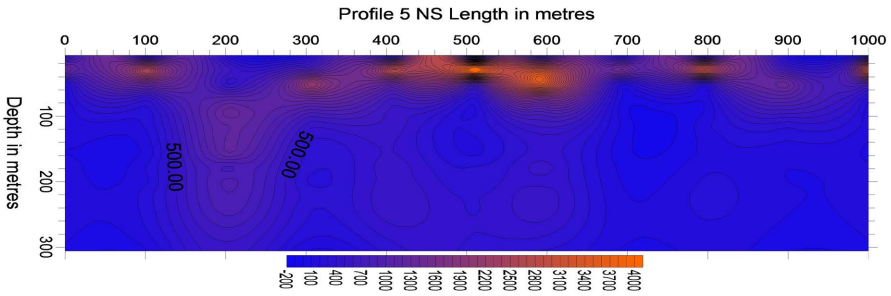

(5)

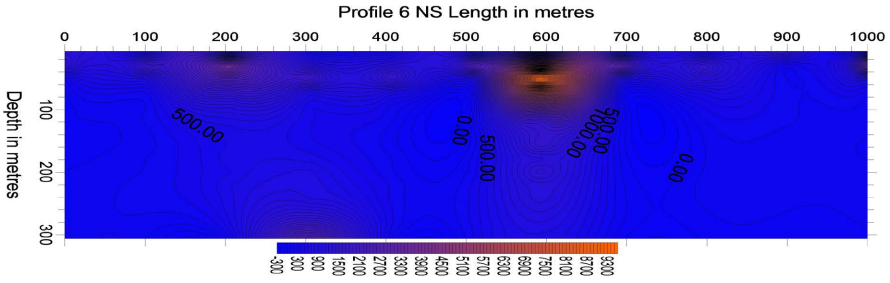
Profile 6 NS Length in metres
Depth in metres

(6)

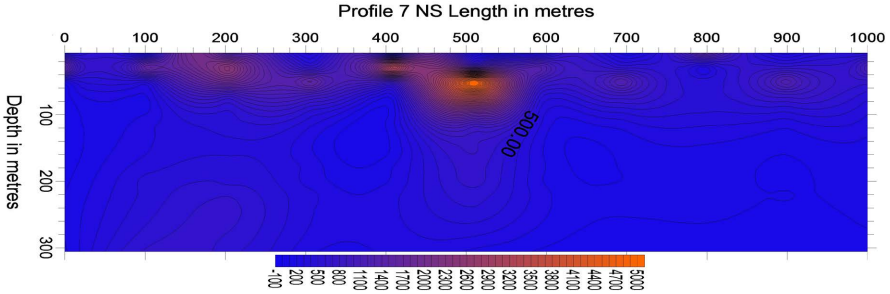
Profile 7 NS Length in metres
Depth in metres

(7)

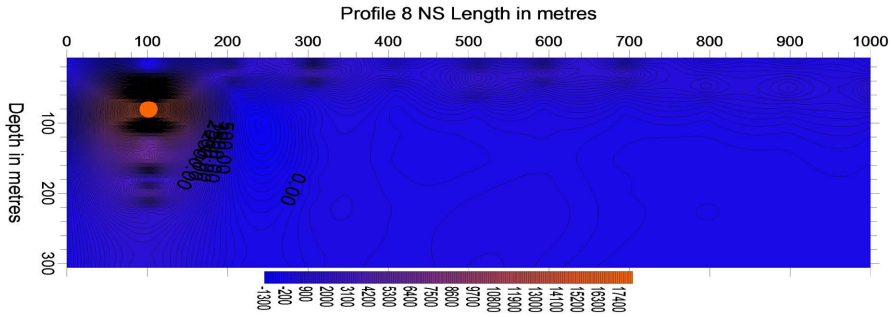
Profile 8 NS Length in metres
Depth in metres

(8)

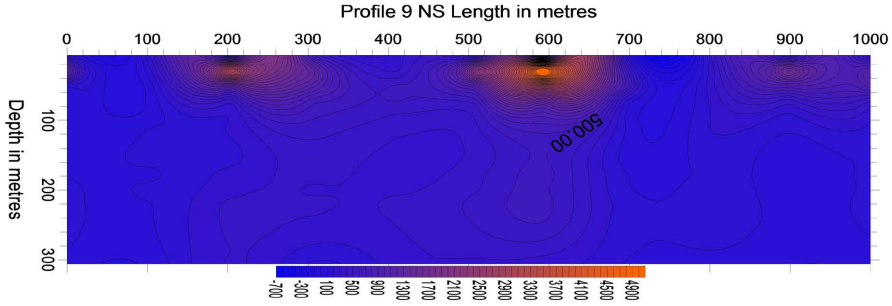
Profile 9 NS Length in metres
Depth in metres

(9)

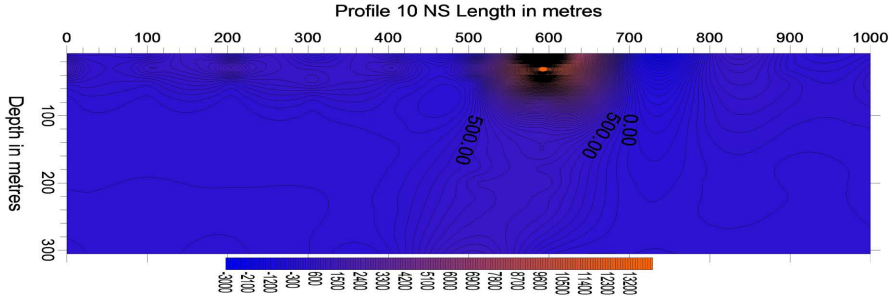
Profile 10 NS Length in metres
Depth in metres

(10)

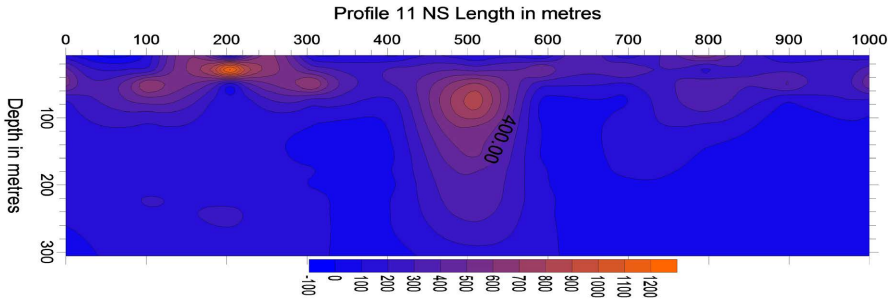
Profile 11 NS Length in metres
0 100 200 300 400 500 600 700 800 900 1000
Depth in metres
100 200 300
400.00
-100 0 100 200 300 400 500 600 700 800 900 1000 1100 1200

(11)

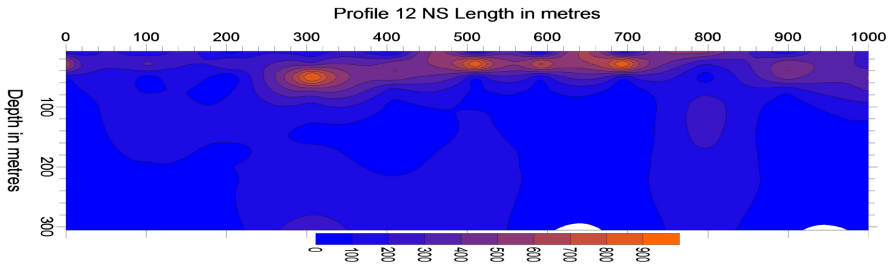
Profile 12 NS Length in metres
0 100 200 300 400 500 600 700 800 900 1000
Depth in metres
100 200 300
0 100 200 300 400 500 600 700 800 900

(12)

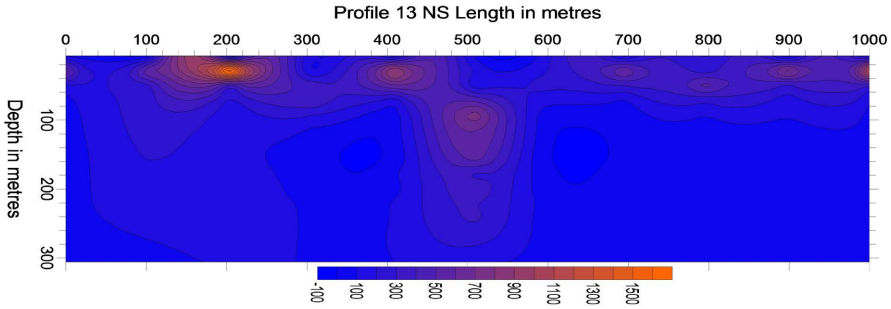
Profile 13 NS Length in metres
0 100 200 300 400 500 600 700 800 900 1000
Depth in metres
100 200 300
-100 100 300 500 700 900 1100 1300 1500

(13)

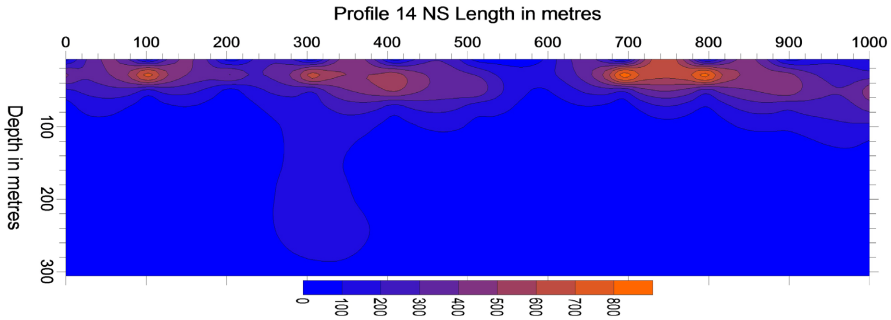
Profile 14 NS Length in metres
0 100 200 300 400 500 600 700 800 900 1000
Depth in metres
100 200 300
0 100 200 300 400 500 600 700 800

(14)

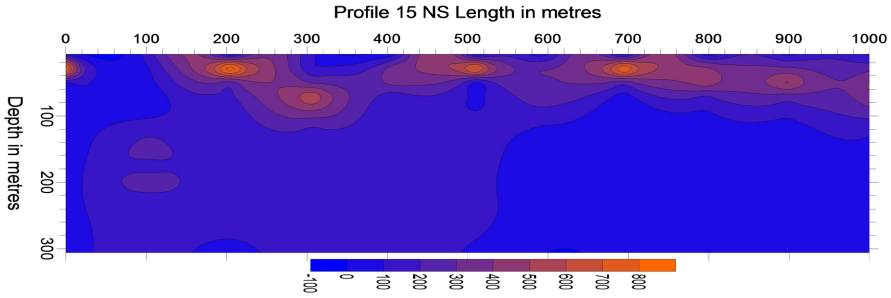
Profile 15 NS Length in metres
0 100 200 300 400 500 600 700 800 900 1000
Depth in metres
100 200 300
-100 0 100 200 300 400 500 600 700 800

(15)

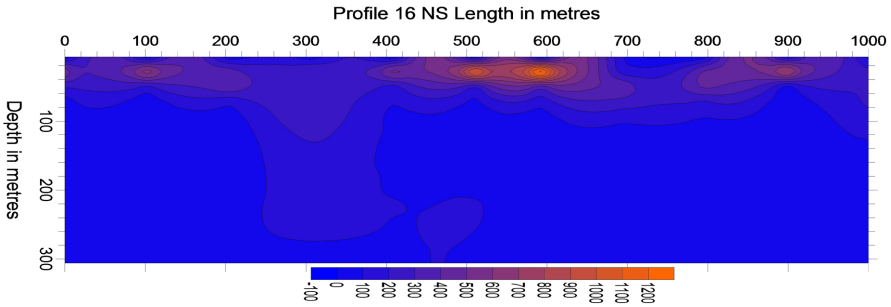

(16)

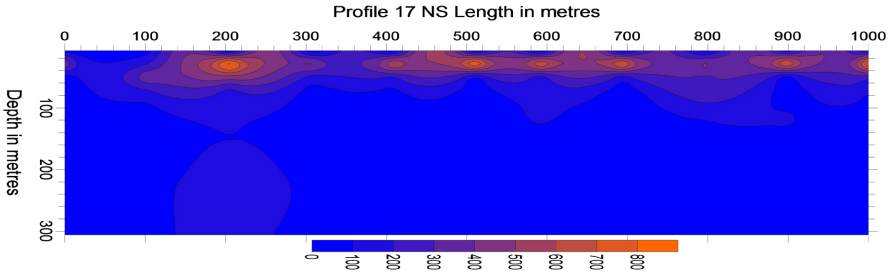

(17)

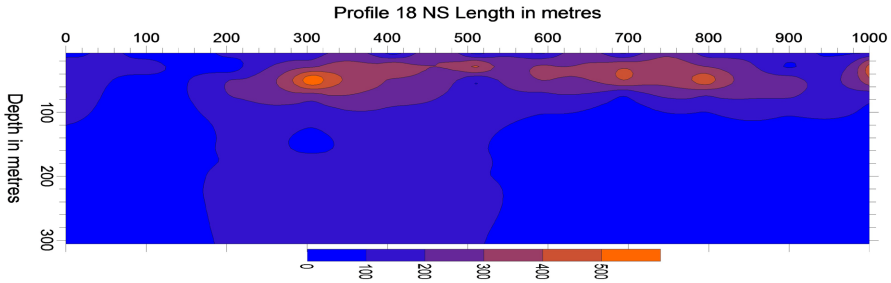

(18)

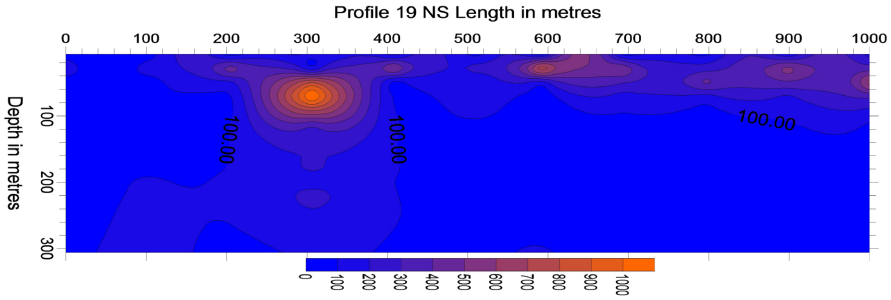

(19)

Figure A1. (1)-(19). Surfer Profiles of combined horizontal VES points' (at 100 m separation) modelled resistivity data.

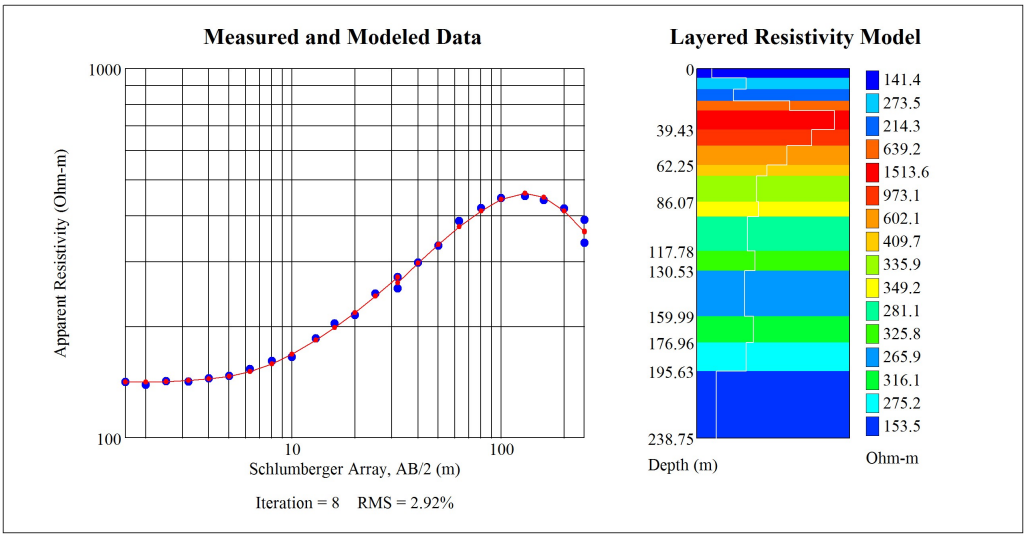
Measured and Modeled Data
Layered Resistivity Model
Apparent Resistivity (Ohm-m)
1000
100
10
100
Schlumberger Array, AB/2 (m)
Iteration = 8 RMS = 2.92%
0
39.43
62.25
86.07
117.78
130.53
159.99
176.96
195.63
238.75
Depth (m)
141.4
273.5
214.3
639.2
1513.6
973.1
602.1
409.7
335.9
349.2
281.1
325.8
265.9
316.1
275.2
153.5
Ohm-m

(a)

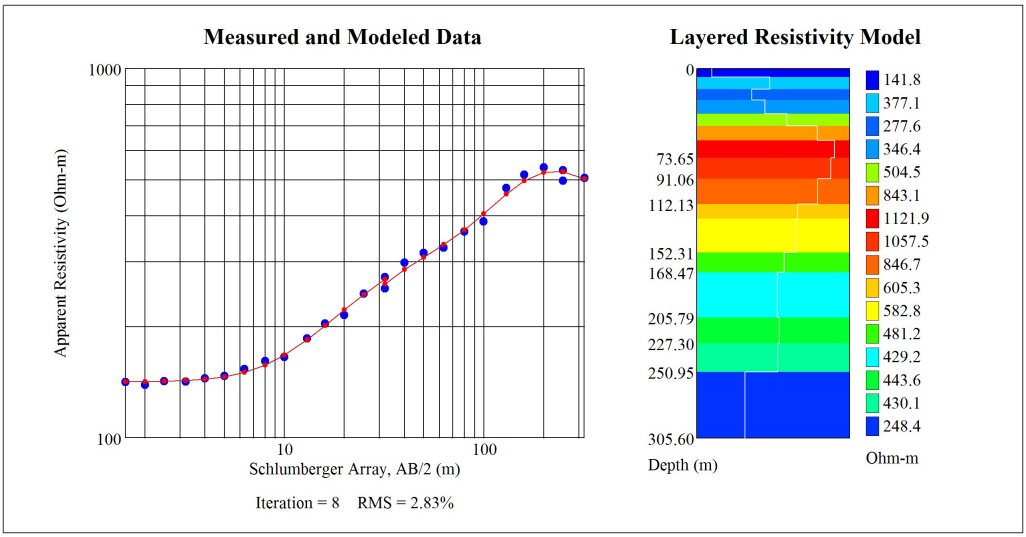
Measured and Modeled Data
Layered Resistivity Model
Apparent Resistivity (Ohm-m)
1000
100
10
100
Schlumberger Array, AB/2 (m)
Iteration = 8 RMS = 2.83%
0
73.65
91.06
112.13
152.31
168.47
205.79
227.30
250.95
305.60
Depth (m)
141.8
377.1
277.6
346.4
504.5
843.1
1121.9
1057.5
846.7
605.3
582.8
481.2
429.2
443.6
430.1
248.4
Ohm-m

(b)

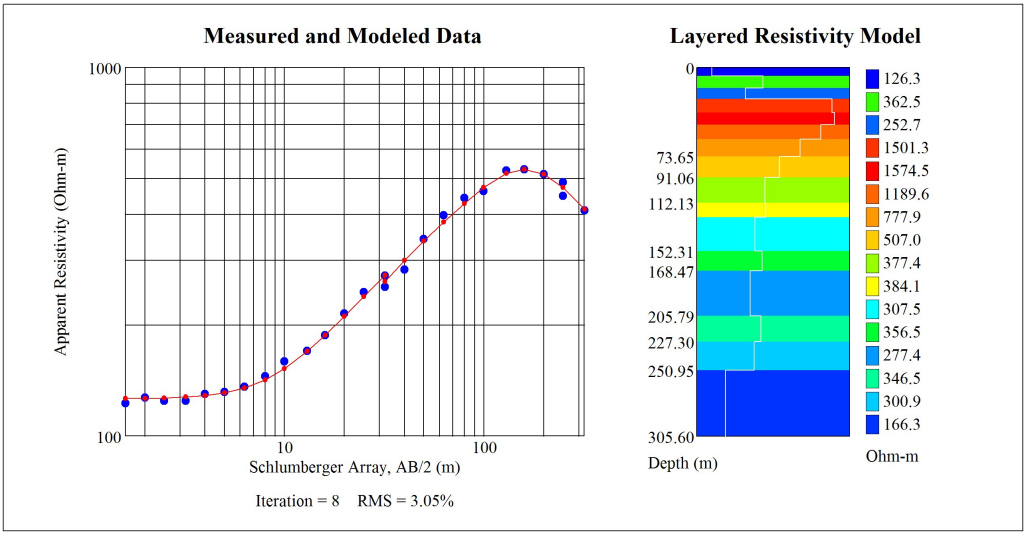
Measured and Modeled Data
Layered Resistivity Model
Apparent Resistivity (Ohm-m)
1000
100
10
100
Schlumberger Array, AB/2 (m)
Iteration = 8 RMS = 3.05%
0
73.65
91.06
112.13
152.31
168.47
205.79
227.30
250.95
305.60
Depth (m)
126.3
362.5
252.7
1501.3
1574.5
1189.6
777.9
507.0
377.4
384.1
307.5
356.5
277.4
346.5
300.9
166.3
Ohm-m

(c)

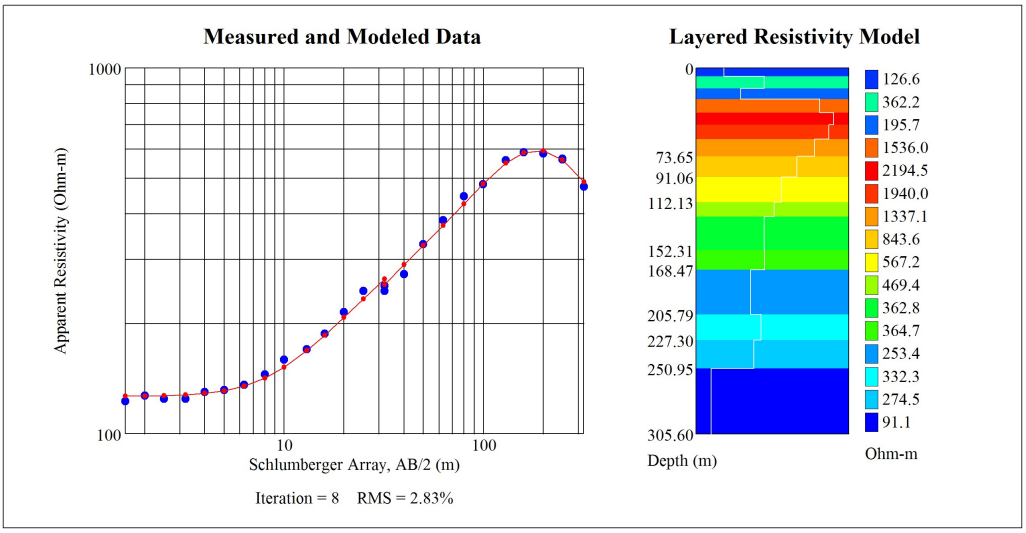
Measured and Modeled Data
Apparent Resistivity (Ohm-m)
1000
100
10
100
Schlumberger Array, AB/2 (m)
Iteration = 8 RMS = 2.83%
Layered Resistivity Model
0
73.65
91.06
112.13
152.31
168.47
205.79
227.30
250.95
305.60
Depth (m)
126.6
362.2
195.7
1536.0
2194.5
1940.0
1337.1
843.6
567.2
469.4
362.8
364.7
253.4
332.3
274.5
91.1
Ohm-m

(d)

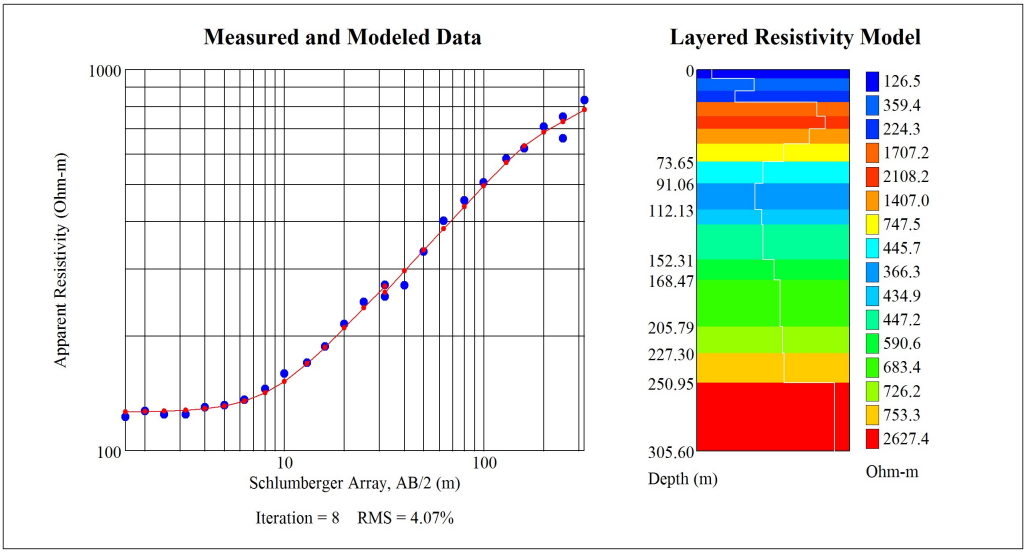
Measured and Modeled Data
Apparent Resistivity (Ohm-m)
1000
100
10
100
Schlumberger Array, AB/2 (m)
Iteration = 8 RMS = 4.07%
Layered Resistivity Model
0
73.65
91.06
112.13
152.31
168.47
205.79
227.30
250.95
305.60
Depth (m)
126.5
359.4
224.3
1707.2
2108.2
1407.0
747.5
445.7
366.3
434.9
447.2
590.6
683.4
726.2
753.3
2627.4
Ohm-m

(e)

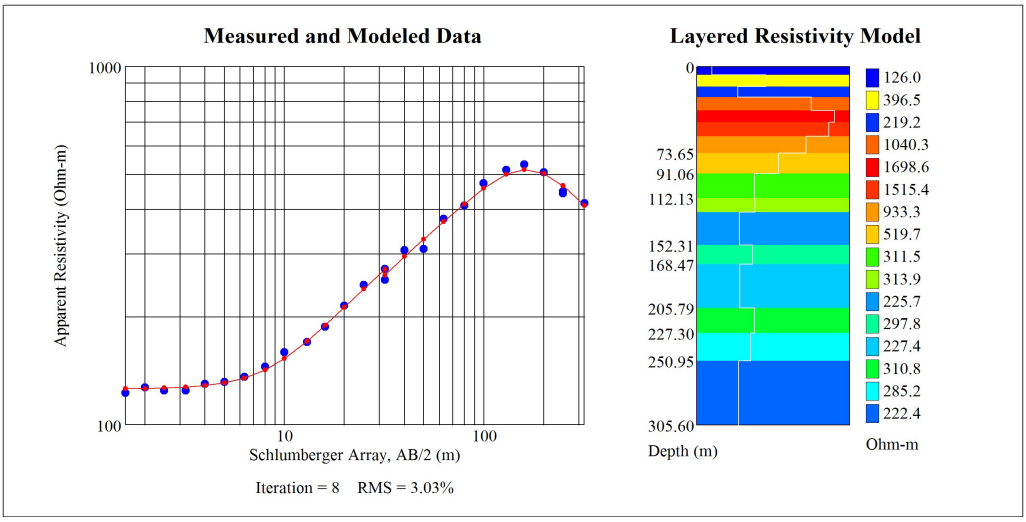
Measured and Modeled Data
Apparent Resistivity (Ohm-m)
1000
100
10
100
Schlumberger Array, AB/2 (m)
Iteration = 8 RMS = 3.03%
Layered Resistivity Model
0
73.65
91.06
112.13
152.31
168.47
205.79
227.30
250.95
305.60
Depth (m)
126.0
396.5
219.2
1040.3
1698.6
1515.4
933.3
519.7
311.5
313.9
225.7
297.8
227.4
310.8
285.2
222.4
Ohm-m

(f)

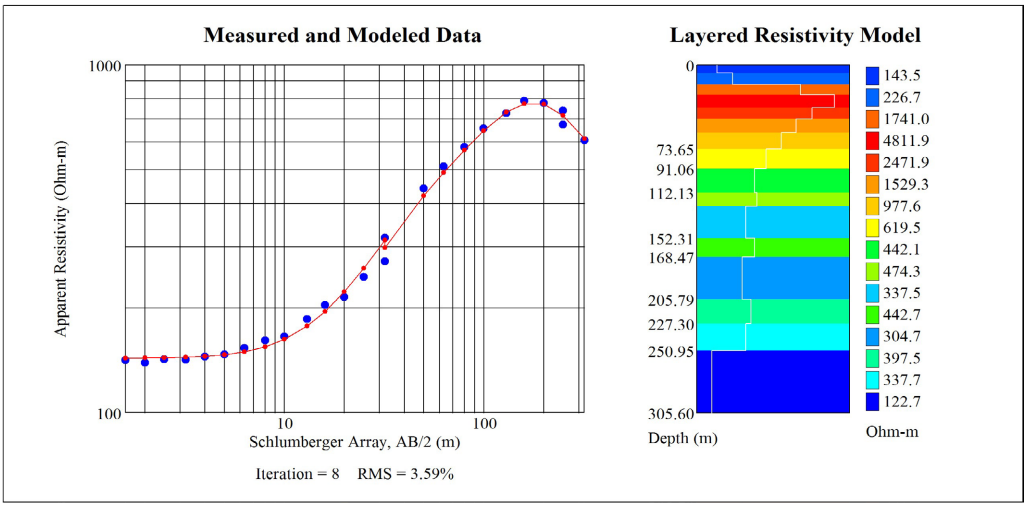

(g)

Figure A2. Profile 4(4) VES 2 - 8 showing measured (blue dots) and modeled (red line and dots) VES data.

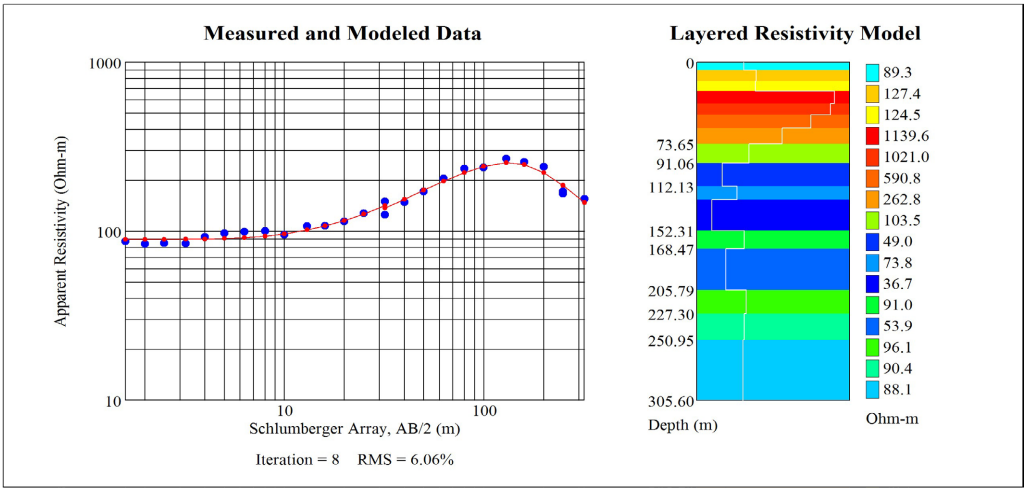

(a)

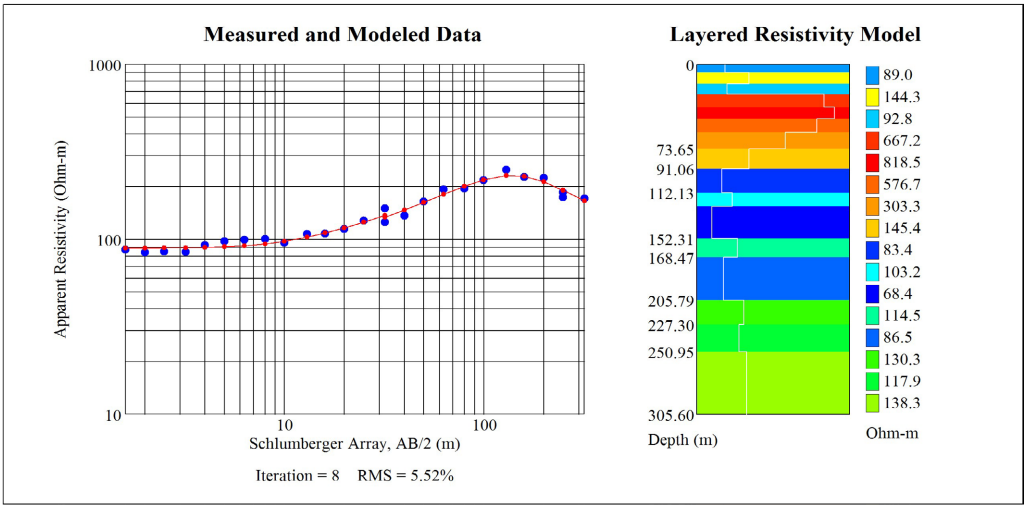

(b)

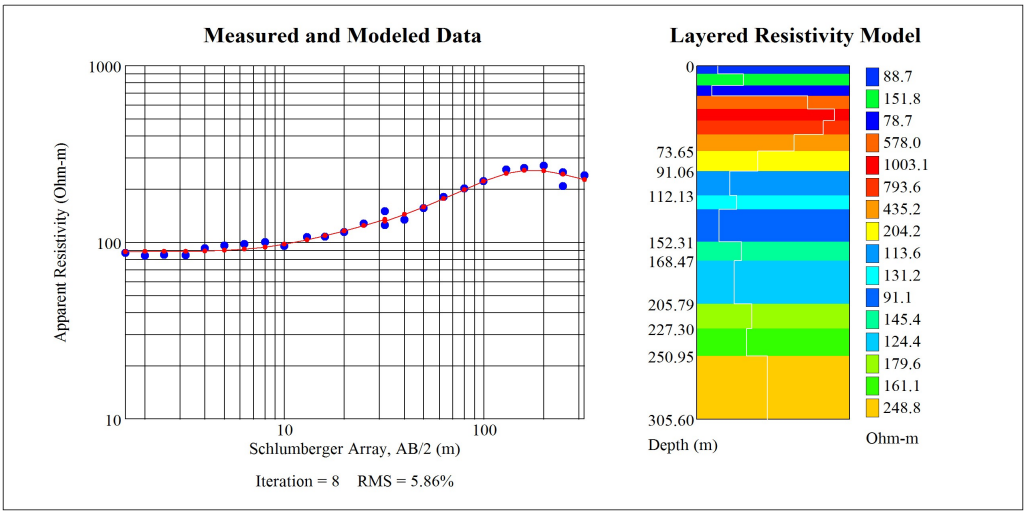

(c)

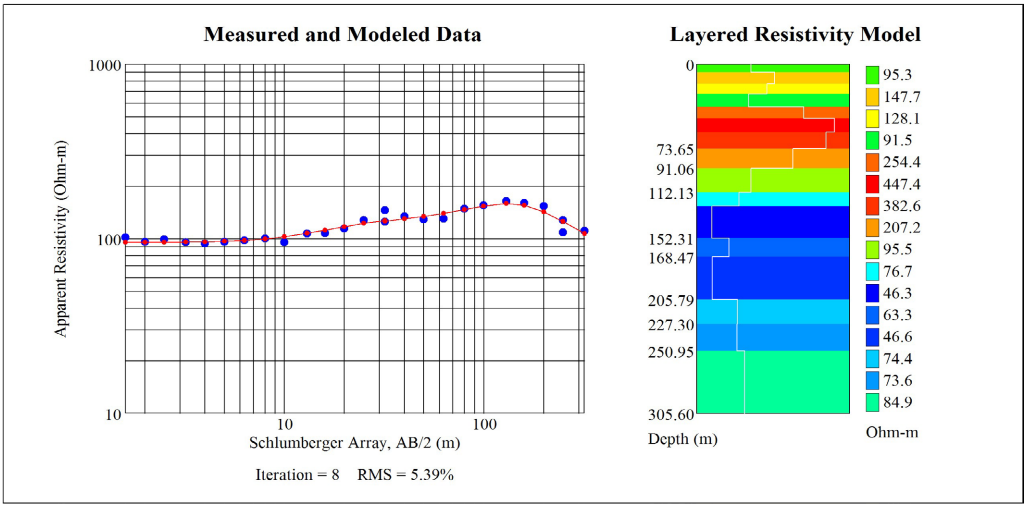

(d)

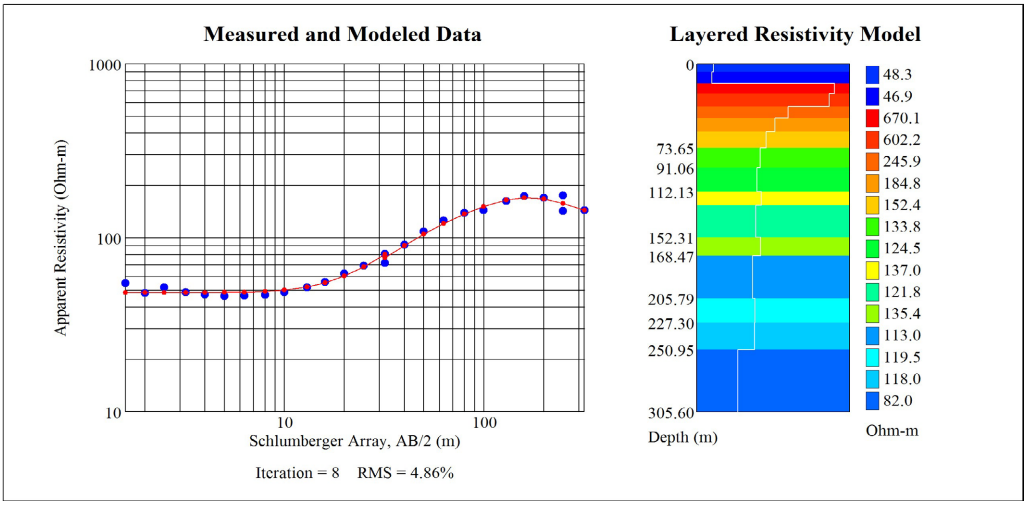

(e)

Figure A3. Profile 4(4) VES 10-14 showing measured (blue dots) and modeled (red line and dots) VES data.